Multiple Particle Tracking in 3-D+t Microscopy: Method and Application to the Tracking of Endocytosed Quantum Dots

Auguste Genovesio, Tim Liedl, Valentina Emiliani, Wolfgang J. Parak, Maité Coppey-Moisan, and Jean-Christophe Olivo-Marin, *Senior Member, IEEE*

***Abstract*—We propose a method to detect and track multiple moving biological spot-like particles showing different kinds of dynamics in image sequences acquired through multidimensional fluorescence microscopy. It enables the extraction and analysis of information such as number, position, speed, movement, and diffusion phases of, e.g., endosomal particles. The method consists of several stages. After a detection stage performed by a three-dimensional (3-D) undecimated wavelet transform, we compute, for each detected spot, several predictions of its future state in the next frame. This is accomplished thanks to an interacting multiple model (IMM) algorithm which includes several models corresponding to different biologically realistic movement types. Tracks are constructed, thereafter, by a data association algorithm based on the maximization of the likelihood of each IMM. The last stage consists of updating the IMM filters in order to compute final estimations for the present image and to improve predictions for the next image. The performances of the method are validated on synthetic image data and used to characterize the 3-D movement of endocytic vesicles containing quantum dots.**

***Index Terms*—Bayesian filtering, cell biology, data association, microscopy, multiple particle tracking, quantum dots.**

I. Introduction

A. Cell Biology and Tracking

AT PRESENT, a considerable part of biological imaging is shifting toward *in vivo* multidimensional fluorescence microscopy, allowing for the visualization of specific biological processes in real time and three dimensions. The introduction of novel microscopy techniques like optical sectioning or confocal microscopy has opened the road to a whole series of research perspectives dedicated to the study of cellular dynamics, and to the links between cellular functions and spatial-temporal localization. For example, nowadays, it is routine in cell biology to film cells, organelles, and pathogens to document infectious disease processes in living systems [1]–[4]. In many such applications, the fluorescently labeled biological objects are visualised as small bright spots superimposed on an uneven background, where a spot is defined as an object which is relatively small and compact and has no clear border, and whose intensity is both diffuse and higher than that of its immediate neighborhood. The reliable quantitative study of motility and dynamic properties requires the computation of parameters like number of spots, position, spatial distribution, movement phases, speed, and diffusion coefficients and, therefore, requires that all the spots in the image sequences are detected and tracked [5], [6]. In the context of living cellular systems, spot tracking can be made particularly difficult by the facts that the dynamics of each spot can change over time or that spots may aggregate temporarily making their appearance change and their proper detection more difficult [6]. Not surprisingly, many biological object motility studies are based on the study of a few hand-picked particles which represent only a small subset of the total [2]. On top of being tedious and time consuming, this type of manual tracking is prone to many errors, highly dependent on operator's skills and perception [1], and can introduce a strong bias in the analysis. It is, therefore, of utmost importance to develop methods to perform the tracking in an automatic, reproducible, and unprejudiced manner.

A large body of work has addressed the tracking of single particles in optical microscopy (see, e.g., [7], for a review) and of multiple spots in military or video imaging [8], [9]. Conversely, relatively little effort has been devoted to multiple particle tracking (MPT) in the cellular and molecular imaging domain [10]–[17]. Conventional MPT methods are based on simple intensity thresholding [10] or local maxima extraction [11] for detecting the spots and on nearest neighbor association (NNA) [10] or constrained NNA [11] to perform the tracking. These methods work well on image sequences showing a limited number of very bright spots on a uniform background, but they fail as soon as the intensity of the spots is not modal, the spots are embedded in noisy images, the density of spots is high, or the displacement of spots is higher than the interspot spacing. In [12], a solution to improve on the previous methods is proposed. It uses the combination of four techniques, namely highly sensitive object detection, fuzzy logic-based dynamic

Manuscript received May 20, 2005; revised October 10, 2005. This work was supported by an IP fellowship and an ANRS AC-14.2 fellowship awarded to A. Genovesio. The associate editor coordinating the review of this manuscript and approving it for publication was Dr. Robert F. Murphy.

A. Genovesio was with the Unité d'Analyse d'Images Quantitative, CNRS URA 2582, Institut Pasteur, 75015 Paris, France, and also with the SIP-CRIP5, Université René Descartes, 75005 Paris, France. He is now with the Institut Pasteur Korea, 136-791 Seoul, Korea (e-mail: auguste.genovesio@pasteur.or.kr).

V. Emiliani was with the Institut Jacques Monod, CNRS, Universités Paris 6 et 7, F-75005 Paris, France. She is now with Laboratoire NeuroPhysiologie et Nouvelles Microscopies, INSERM U603, CNRS FRE 2500, Université Paris 5, F-75006 Paris, France (e-mail: valentina.emiliani@univ-paris5.fr).

M. Coppey-Moisan is with the Institut Jacques Monod, CNRS, Universités Paris 6 et 7, 75005 Paris, France (e-mail: e coppey@ijm.jussieu.fr).

T. Liedl and W. J. Parak are with the Center for Nanoscience (CeNS), Ludwig-Maximilians Universität München, D-80799 Munich, Germany (e@ijm.jussieu.frmail: tim.liedl; wolfgang.parak@physik.uni-muenchen.de).

J.-C. Olivo-Marin is with the Unité d'Analyse d'Images Quantitative, CNRS URA 2582, Institut Pasteur, 75015 Paris, France (jcolivo@pasteur.fr).

Digital Object Identifier 10.1109/TIP.2006.872323

object tracking, computer graphical visualization, and measurement in time space. Although this method is effective when working with well separated objects, it shows some limitations in keeping up with aggregating ones. A more robust algorithm is presented in [13], [14]. Based on ideas from operational research and graph theory, it proceeds in four steps: particle detection; generation of candidate matches, i.e., a set of possible displacement vectors between successive frames; scoring of candidate matches; and selection of the candidate subset with maximum global score and no topological ambiguity. This method, however, relies on a number of heuristic rules and on *a priori* information on the movements of objects to be effective. Also, the extension and application of the algorithm to four-dimensional data has not been reported.

Here, we report a method to perform the detection and the tracking of microscopic spots directly on four dimensional (3-D+t) image data. It extends and outperforms our previous work [15]–[17] by being able to detect with high accuracy multiple biological objects moving in three-dimensional (3-D) space and by incorporating the possibility to follow moving spots switching between different dynamics characteristics. Our method decouples the detection and the tracking processes and is based on a two step procedure: first, the objects are detected in the image stacks thanks to a procedure based on a 3-D wavelet transform; then, the tracking is performed within a Bayesian framework where each object is represented by a state vector evolving according to biologically realistic dynamic models. The main advantage of wavelet-based detection is to be robust to the local variation of contrast and to the imaging noise. The Bayesian tracking allows us to predict the new position of a spot knowing its past positions and increases the reliability of the data association step.

B. Bayesian Multitarget Tracking

Bayesian multitarget tracking methods consist of filtering successive measurements coming from a detector. They are generally split into two subprocedures: Bayesian filtering and data association. The generic formulation of Bayesian filtering is to compute the successive posterior densities $p(\mathbf{x}_t|\mathbf{m}_{1:t})$ from the set of already detected measurements $\mathbf{m}_{1:t} = \{\mathbf{m}_1, \ldots, \mathbf{m}_t\}$ and the following system:

$$\mathbf{x}_t|\mathbf{x}_{t-1} \sim p(\mathbf{x}_t|\mathbf{x}_{t-1}) \tag{1}$$

$$\mathbf{m}_t|\mathbf{x}_t \sim p(\mathbf{m}_t|\mathbf{x}_t) \tag{2}$$

where $\mathbf{m}_t$ is the measurement of a hidden evolving signal $\mathbf{x}_t$ obtained at each time step through the observation process (2) with a time prior (i.e., the assumption made on the evolution of state $\mathbf{x}_t$ through time) given by (1). The exact solution to this problem is constructed in two steps. First, a prediction of the prior density is computed by

$$p(\mathbf{x}_t|\mathbf{m}_{1:t-1}) = \int p(\mathbf{x}_t|\mathbf{x}_{t-1})p(\mathbf{x}_{t-1}|\mathbf{m}_{t-1})d\mathbf{x}_{t-1} \tag{3}$$

based on a Markov assumption on the process $\mathbf{x}_t$. Then, from (3), and thanks to the Bayes rule, the update of the posterior density is obtained as

$$p(\mathbf{x}_t|\mathbf{m}_{1:t}) = \frac{p(\mathbf{m}_t|\mathbf{x}_t)p(\mathbf{x}_t|\mathbf{m}_{1:t-1})}{\int p(\mathbf{m}_t|\mathbf{x}_t)p(\mathbf{x}_t|\mathbf{m}_{1:t-1})d\mathbf{x}_t}. \tag{4}$$

In practice, however, this scheme cannot be applied because the multidimensional integral in (3) and (4) cannot be computed in the general case. Several solutions have been proposed to make the problem tractable by imposing some constraints on the density distributions. Depending on the constraints and on the *a priori* information available on the system, the solution to the posterior density can be optimal like in the case of the well known Kalman filter (KF) (optimal in the MMSE sense for a linear Gaussian density) [18], suboptimal (yet more efficient to approximate the posterior density in nonlinear/non-Gaussian cases) in the case of the extended Kalman filter (EKF) [8], the Kalman unscented filter [19], and the particle filter (PF) [20]–[22] or exact in the case of the grid-based filter (GBF) [22]. All the previous filters are bound to use just one dynamic model in their scheme, however, which is problematic when the objects' dynamics vary with time as it is the case with biological objects. The interacting multiple models (IMMs) filter [23], [24], instead, has been designed, first in the context of radar imaging, with the capability to have different models in parallel, and to select and switch to the model which is more accurate to represent the movement during a given period. The IMM has the additional ability to rapidly self adapt to transitions. This altogether makes the IMM the best choice for our application and here we report its first application to biological imaging and propose several models adapted to biological object dynamics.

Data association is a crucial step when tracking several particles in the presence of clutter. Indeed, as the detection may miss or wrongly detect objects, naive association methods will create inconsistent associations leading to disconnected trajectories in subsequent images. Among the numereous methods that have been developed to tackle this problem, the most popular algorithms are the nearest neighbor (NN) [8], the joint probabilistic data association (JPDA) [9], [25], and the multihypothesis tracking (MHT) [26], [27], but none of them is really adapted to our specific needs. The NN is very sensitive to noise and performs quite badly even with moderate noise levels. The JPDA, which computes the joint probability of all the different associations, requires the number of objects be known in advance and remain constant during the sequence, a condition not met in our applications where the number of particles varies in time. The MHT algorithm is very compelling conceptually as it is based on the dynamic computation of the probability tree describing all possible associations of particles over time. Notwithstanding its theoretical advantages, it rapidly becomes intractable because the complexity increases exponentially with the number of tracked objects. There are no established and reliable implementations for applications where the number of considered objects exceeds a few units; thus, the MHT could not satisfy our demand of being able to handle several tens or hundreds of particles. We, therefore, propose an association method based on a maximum likelihood approach that has proved to achieve better results than an optimal NN (i.e., that minimizes the distance sum) approach with a reasonable complexity.

C. Tracking of Vesicles Labeled With Quantum Dots (QDs)

To validate the performances of our method on real biological microscopic data, we have tracked endocytic vesicles to monitor

the effect of the overexpression of the protein tau in the microtubule dependent transport of single vesicles in living Hela cells. Vesicles were marked with red fluorescent inorganic CdSe/ZnS QDs. We compared the results obtained in nontreated cells with those in cells transfected with tau-GFP. Our results are in agreement with the work from another team [28] where the analysis of microscopy data was done manually and confirm that tau does not alter the speed of motors but reduces the mean 3-D trajectory range of endocytic vesicles [28]. This confirmation is very encouraging and it opens the way to an increased use of automatic tracking methods to analyze complex biological image sequences.

D. Organization of the Paper

The paper is organized as follows. In Section II, we briefly describe the detection method. Section III presents the different algorithms used to perform the tracking together with an evaluation of the IMM filter. The results achieved by the presented method are then evaluated in Section IV, where results are presented both for synthetic sequences and for real biological microscopy sequences.

II. Spot Detection

We have developed a spot detection method which is based on a shift invariant 3-D discrete wavelet transformation of the image stacks and on the selective filtering of wavelet coefficients. This method extends our previous work on two-dimensional (2-D) images [29] and presents several advantages over simpler segmentation methods: 1) It is robust to local variations of contrast and to the imaging noise. 2) It allows us to efficiently segment fluorescent spots imbedded in noisy images such as those acquired with real-time confocal microscopy. 3) It enables to select spots of a specified size. 4) It allows us to discard low-frequency objects that are present in the background and that would hinder any conventional threshold based method. 5) It allows us to take into account the difference in resolution along the z axis by selecting filters of different length in x, y, and z (typically, we use a B3-spline filter [30] in the x and y directions and a Haar filter in z). Given an input noisy image stack $Y = I + n$, and its wavelet transformation $W^Y = W^I + W^n$, wavelet thresholding is performed with Jeffreys' noninformative threshold t_{n_i} [31] as an estimation of the significance of wavelet coefficient $W_i^Y(x,y,z)$ at a given scale i and position (x,y,z)

$$t_{n\_i}\left(W_i^Y(x,y,z)\right) = \left\{W_i^Y(x,y,z) : W_i^Y(x,y,z) \geq \frac{\left(\left(W_i^Y(x,y,z)\right)^2 - 3\sigma_i^2\right)_+}{W_i^Y(x,y,z)}, 0\right\} \quad (5)$$

where σ_i is the standard deviation of noise at scale i in the wavelet domain (we assume that the noise is stationary at each scale). The choice of this threshold function is motivated by the fact that other functions like Donoho's hard or soft threshold [32] are too drastic in cutting wavelet coefficients and do not allow for weak objects to be detected. To characterize the spots, we compute a correlation image stack $P_s(x,y,z)$ which is the direct multiplication of s denoised wavelet image stacks corresponding to the selected scales

$$P_s(x,y,z) = \prod_{i=j_1}^{j_s} W_i^Y(x,y,z)_+. \quad (6)$$

The correlation reduces the remaining noise and has significant values only at locations that correspond potentially to spots. After binarization, each connected component (spot) in P_s is extracted to create a measurement vector $\mathbf{m}_t = [x_t, y_t, z_t, v_t, i_t]^T$ consisting of its location (x,y,z), volume v and mean intensity i at time t [16]. This vector is used in the following steps to create the spot trajectories. An example of detection result is presented in Fig. 1.

III. Tracking

To establish the trajectories, it is necessary to link the successive vectors $\mathbf{m}_t$ representing the set of available measurements on the system. To avoid creating inconsistent associations leading to disconnected trajectories in subsequent images, two important facts have to be taken into consideration. 1) A detection does not necessarily correspond to a real object but could have been generated by clutter, and 2) an object might have been missed (not detected). To properly handle these situations, the tracking algorithm has to be able either to terminate a track if a wrong measurement has been generated or to provide a predicted measurement that will be used to temporarily retain a track in case a real measurement can be assigned in the subsequent images. Another major problem is that biological object dynamics vary abruptly and frequently over time leading to association problems. To handle this, we use an IMM filter with several dynamic models that allow us to achieve a good prediction during the transition between movements.

A. IMM Filter

The IMM filter is a Bayesian state estimation algorithm for a system represented by Markovian switching coefficients. It was originally developed by Blom [24] and used by Blom and Bar Shalom [23] first in the context of radar imaging. We recall, here, the principles of this method. We want to compute the posterior density $p(\mathbf{x}_t|\mathbf{m}_{1:t})$ as a weighted sum of gaussians $N(\mathbf{x}_t; \hat{\mathbf{x}}_{t|t}^j, \mathbf{P}_{t|t}^j)$ based on the assumption that the generic system presented in (1) and (2) is reduced to a set of switching linear models with additive Gaussian noises and, thus, has the form

$$\mathbf{x}_t = \mathbf{F}_t^j \mathbf{x}_{t-1} + \mathbf{w}_t^j \quad (7)$$

$$\mathbf{m}_t = \mathbf{H}_t^j \mathbf{x}_t + \mathbf{v}_t^j \quad (8)$$

where $\mathbf{x}_t$ is the system state vector at time t, $\mathbf{m}_t$ is the measurement vector at time t, and $\mathbf{F}_t^j$ is the state transition matrix for the event M_t^j (event defined as "model j is active at time t"). $\mathbf{H}_t^j$ is the observation matrix for M_t^j. $\mathbf{w}_t^j$ and $\mathbf{v}_t^j$ are the process and measurement noise vectors, that are mutually uncorrelated zero-mean white Gaussian processes with covariance matrices $\mathbf{Q}_t^j$ and $\mathbf{R}_t^j$. We denote by $j \in \{1, \ldots, r\}$ the index of the r models.

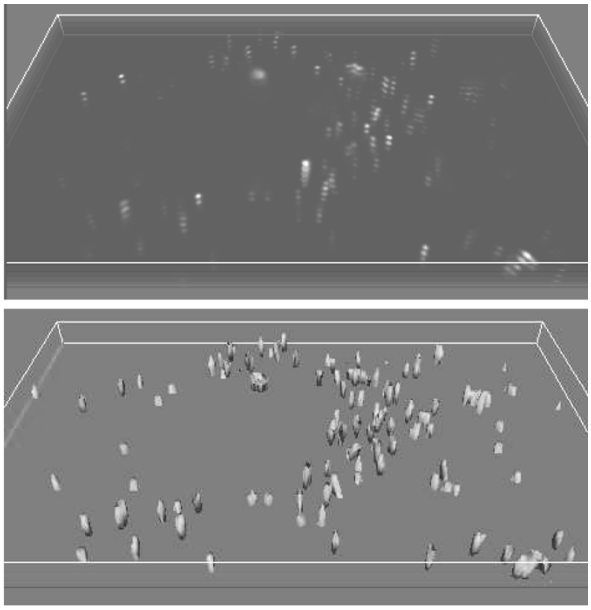

Fig. 1. Detection of vesicles in 3-D. (a) original real 3-D microscopy image stack showing QD-labeled vesicles. (b) Result of the detection by the proposed method.

The switching between models is governed by a finite state Markov chain with probabilities $p_{ij} = Pr\{M_t^j | M_{t-1}^i\}$ of switching from M_{t-1}^i to M_t^j. The optimal approach for filtering the system state would be that every possible sequence of models be considered, thus involving an exponentially increasing number of filters. To make the computation tractable, the IMM estimator [9], [23] uses instead an approximation which is to consider the two most recent sampling periods only. The IMM estimator is a recursive process consisting of several steps at each iteration.

First, the initial input for each KF j at time step t (also called the mixed estimated state and covariance, and noted with a "0" superscript) is computed by

$$\hat{\mathbf{x}}_{t-1|t-1}^{0j} = \sum_{i=1}^{r} \mu_{t-1|t-1}^{i|j} \hat{\mathbf{x}}_{t-1|t-1}^{i} \tag{9}$$

$$\mathbf{P}_{t-1|t-1}^{0j} = \sum_{i=1}^{r} \mu_{t-1|t-1}^{i|j} \left\{ \mathbf{P}_{t-1|t-1}^{i} + \left[\hat{\mathbf{x}}_{t-1|t-1}^{i} - \hat{\mathbf{x}}_{t-1|t-1}^{0j} \right] \times \left[\hat{\mathbf{x}}_{t-1|t-1}^{i} - \hat{\mathbf{x}}_{t-1|t-1}^{0j} \right]^T \right\} \tag{10}$$

where the conditional model probabilities are given by

$$\mu_{t-1|t-1}^{i|j} = Pr\left\{ M_{t-1}^{i} | M_t^j, \mathbf{m}_{1:t-1} \right\} = \frac{1}{\mu_{t|t-1}^{j}} p_{ij} \mu_{t-1|t-1}^{i} \tag{11}$$

and the predicted model probability by

$$\mu_{t|t-1}^{j} = Pr\left\{ M_t^i | \mathbf{m}_{1:t-1} \right\} = \sum_{i=1}^{r} p_{ij} \mu_{t-1|t-1}^{i}. \tag{12}$$

Second, for each filter, the state prediction $\hat{\mathbf{x}}_{t|t-1}^{j}$ and covariance prediction $\mathbf{P}_{t|t-1}^{j}$ are computed for each model j with the standard KF equations [8], [18] with initial values given by (9) and (10). These predictions are used in the association step which provides to each track the measurement $\mathbf{m}_t$ that corresponds to the best global solution as detailed in Section III-D and from which it is possible to compute the state estimation $\hat{\mathbf{x}}_{t|t}^{j}$ and the covariance estimation $\mathbf{P}_{t|t}^{j}$. These estimations can be computed in parallel for each model as they are totally independent from each other.

Third, as the innovation is considered to be a $\dim(\mathbf{m})$-dimensional Gaussian statistic with zero mean, it follows that the likelihood of each filter matched to M_t^j is given by

$$\Lambda_t^j = f\left(\mathbf{m}_t | M_t^j, \mathbf{m}_{1:t-1} \right) = \frac{1}{\sqrt{\det\left[2\pi \mathbf{S}_t^j \right]}} \exp\left\{ \frac{-1}{2} \left[\tilde{\mathbf{m}}_t^j \right]^T \left[\mathbf{S}_t^j \right]^{-1} \tilde{\mathbf{m}}_t^j \right\} \tag{13}$$

where $\tilde{\mathbf{m}}_t^j = [\mathbf{m}_t - \mathbf{m}_{t|t-1}^j]$ and $\mathbf{S}_t^j$ are, respectively, the innovation and the covariance of the innovation of KF j.

Then, the probability for M_t^j is

$$\mu_{t|t}^{j} = Pr\left\{ M_t^j | m_{1:t} \right\} = \frac{1}{\sum_{i=1}^{r} \mu_{t|t-1}^{i} \Lambda_t^i} \mu_{t|t-1}^{j} \Lambda_t^j \tag{14}$$

and the combined state estimate and covariance are

$$\hat{\mathbf{x}}_{t|t} = \sum_{j=1}^{r} \mu_{t|t}^{j} \hat{\mathbf{x}}_{t|t}^{j} \tag{15}$$

$$\mathbf{P}_{t|t} = \sum_{j=1}^{r} \mu_{t|t}^{j} \left\{ \mathbf{P}_{t|t}^{j} + \left[\hat{\mathbf{x}}_{t|t}^{j} - \hat{\mathbf{x}}_{t|t} \right] \left[\hat{\mathbf{x}}_{t|t}^{j} - \hat{\mathbf{x}}_{t|t} \right]^T \right\}. \tag{16}$$

B. Capability of the IMM

To illustrate the capability of the IMM to self-adapt to different movement types as well as to the switching between them, we simulated a one dimensional signal x that switches between two linear models. To simulate the noise and the measurement process z, the signal was corrupted by sequentially adding two Gaussian noises with different variance to the original signal. The measurement z was then filtered back independently by a KF using one of the models and an IMM filter with both models being active. Fig. 2 shows that the IMM produces an estimation that is globally much more reliable than the KF. Conversely, the KF is more efficient on the local portions of the signal ($t = 0$ to 70) that corresponds to its model, which is well in accordance with the fact that the KF is the optimum solution for a linear Gaussian system. Fig. 3 illustrates that switching between models is tractable thanks to the multimodal posterior density which is computed by the IMM.

C. Proposed Dynamic Models

To adapt the IMM to biological imaging, we propose to use three different models of dynamics: random walk (RW), first-order linear extrapolation (FLE), and second-order linear extrapolation (SLE). They model Brownian motion and directed movement with constant speed or acceleration, which are representative modes of motion encountered in biology [3]. We make the additional realistic hypothesis that, during movement, the biological objects can switch abruptly between the three models. This description is complemented by the hypothesis that the

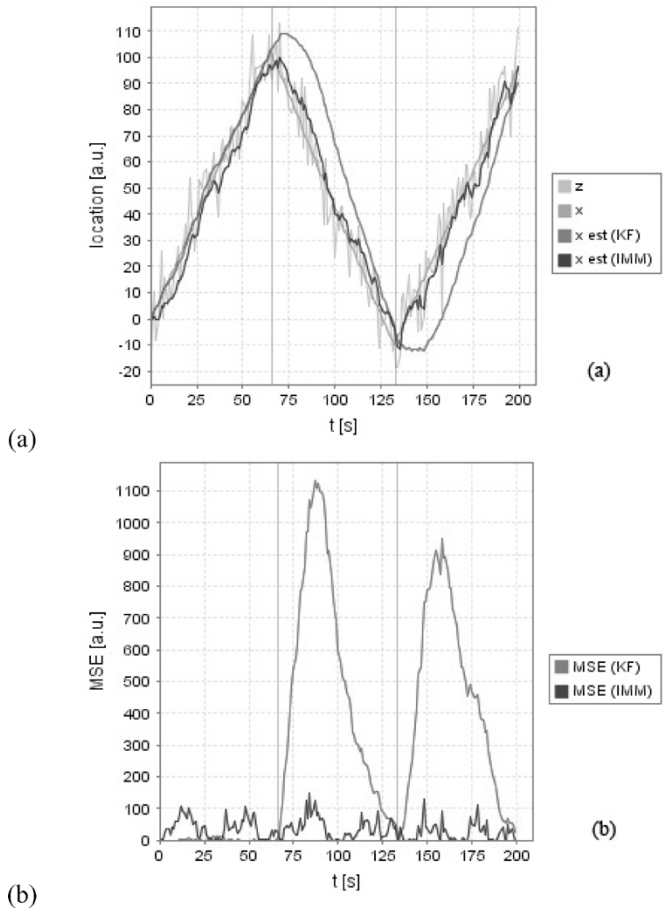

Fig. 2. (a) (Hidden) Signal x is estimated with a KF and an IMM filter from noisy measurements z. We can see that the KF fails to adapt itself to the abrupt switching between models. On the contrary, the IMM filter switches from one model to another with a lower error. (b) Comparison of the mean-square error (MSE) of KF and IMM estimations.

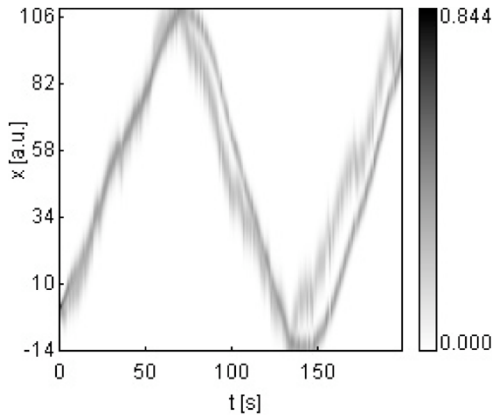

Fig. 3. Reconstructed propagation of $p(\mathbf{x}_t|\mathbf{m}_t)$ in the example of Fig. 2 from IMM parameters. As expected, the density becomes bi-modal when the signal switches from one model to another one.

volume v_t and the mean intensity i_t of each spot remain approximately constant with an additive gaussian noise. By writing the state vector as a concatenation of three successive locations

$$\mathbf{x}_t = [x_t, y_t, z_t, v_t, i_t, x_{t-1}, y_{t-1}, z_{t-1}, x_{t-2}, y_{t-2}, z_{t-2}]^T \tag{17}$$

each of three models can be represented by a linear application, thus enabling us to take into account in the IMM up to three consecutive vector states while still lying within a Markov process of order 1. The three models are as follows.

1) The RW model which makes the assumption that the next state is defined by the previous state and an additive Gaussian noise

$$\mathbf{F}^1 = \left[\begin{array}{ccccc|cccccc} 1&0&0&0&0&0&0&0&0&0&0\\ 0&1&0&0&0&0&0&0&0&0&0\\ 0&0&1&0&0&0&0&0&0&0&0\\ 0&0&0&1&0&0&0&0&0&0&0\\ 0&0&0&0&1&0&0&0&0&0&0\\ \hline 1&0&0&0&0&0&0&0&0&0&0\\ 0&1&0&0&0&0&0&0&0&0&0\\ 0&0&1&0&0&0&0&0&0&0&0\\ 0&0&0&0&0&1&0&0&0&0&0\\ 0&0&0&0&0&0&1&0&0&0&0\\ 0&0&0&0&0&0&0&1&0&0&0 \end{array}\right].$$

2) The FLE model which makes the assumption that the next state is defined by the linear extrapolation of the last two 3-D locations while keeping the same intensity and volume

$$\mathbf{F}^2 = \left[\begin{array}{cccccccc|ccc} 2&0&0&0&0&-1&0&0&0&0&0\\ 0&2&0&0&0&0&-1&0&0&0&0\\ 0&0&2&0&0&0&0&-1&0&0&0\\ 0&0&0&1&0&0&0&0&0&0&0\\ 0&0&0&0&1&0&0&0&0&0&0\\ 1&0&0&0&0&0&0&0&0&0&0\\ 0&1&0&0&0&0&0&0&0&0&0\\ \hline 0&0&1&0&0&0&0&0&0&0&0\\ \hline 0&0&0&0&0&1&0&0&0&0&0\\ 0&0&0&0&0&0&1&0&0&0&0\\ 0&0&0&0&0&0&0&1&0&0&0 \end{array}\right].$$

3) The SLE model, which makes the assumption that the next state is defined by the linear extrapolation of the three last 3-D locations while keeping the same intensity and volume

$$\mathbf{F}^3 = \left[\begin{array}{ccccccccccc} 3&0&0&0&0&-3&0&0&1&0&0\\ 0&3&0&0&0&0&-3&0&0&1&0\\ 0&0&3&0&0&0&0&-3&0&0&1\\ 0&0&0&1&0&0&0&0&0&0&0\\ 0&0&0&0&1&0&0&0&0&0&0\\ 1&0&0&0&0&0&0&0&0&0&0\\ 0&1&0&0&0&0&0&0&0&0&0\\ 0&0&1&0&0&0&0&0&0&0&0\\ 0&0&0&0&0&1&0&0&0&0&0\\ 0&0&0&0&0&0&1&0&0&0&0\\ 0&0&0&0&0&0&0&1&0&0&0 \end{array}\right].$$

The observation model $\mathbf{H}$ related to the measurement vector (II) is common to all three models

$$\mathbf{H} = \begin{bmatrix} 1&0&0&0&0&0&0&0&0&0&0\\ 0&1&0&0&0&0&0&0&0&0&0\\ 0&0&1&0&0&0&0&0&0&0&0\\ 0&0&0&1&0&0&0&0&0&0&0\\ 0&0&0&0&1&0&0&0&0&0&0 \end{bmatrix}. \tag{18}$$

D. Association

To form the correct tracks, it is necessary thereafter to go through an association stage. This consists in finding the best assignment between the new measurements obtained at the detection step and the predicted measurements provided by the IMMs. The assignment is made as follows. First, we compute the maximum likelihood of the innovation among the models in each IMM that we denote $\Lambda_t^{\max}(i,l)$. That is to say, for each measurement $\mathbf{m_i}(t)$, $i \in \{1,\cdots,m\}$ and each IMM filter l, $l \in \{1,\cdots,n\}$, we find the value which maximizes (13). Each of them is used to form the following matrix:

$$\mathbf{L} = \begin{bmatrix} & \vdots & \\ \cdots & \Lambda_t^{\max}(i,l) & \cdots \\ & \vdots & \end{bmatrix}. \tag{19}$$

This is done only for the measurements which are within the validation gates (i.e., the Mahalanobis distance between predicted and estimated measurements is inferior to the square of a given g which is determined from a $\chi^2_{\dim(m)}$ table as corresponding to a gating probability chosen to be at least 0.95).

The assignments $(a_0,\ldots,a_{\min(n,m)})$ are then found according to the following:

$$a_k = (i_k, l_k) = \arg \max_{(i,l)\in \mathbf{J}_k} \mathbf{L}(i,l) \tag{20}$$

with

$$\begin{cases} \mathbf{J}_0 = \{(i,l), i \in \{1,\cdots,m\}, l \in \{1,\cdots,n\}\} \\ \mathbf{J}_{k+1} = \mathbf{J}_k \setminus \{(i,l), \{i = i_k\} \cup \{l = j_k\}\} \end{cases}. \tag{21}$$

The search for assignments stops when $\mathbf{J}_k = \{\emptyset\}$. Even though this assignment technique is sub optimal in a global sense, i.e., it may occur that

$$\exists \{b_0,\ldots,b_{\min(n,m)}\}, \quad \sum_k \mathbf{L}(a_k) < \sum_k \mathbf{L}(b_k) \tag{22}$$

it produces in our application context much better results than an algorithm for optimal assignment between two sets like, for example, the Jonker and Volgenant algorithm [33]. When dealing with our data, the JVC algorithm was not able to output correct associations on more than the first five time points in a sequence. This can be explained by the fact that the JVC algorithm requires the cardinality of the two sets be equal, an assumption that is not met in our case as we are trying to resolve an ill-posed problem where the number of predicted measurements never equals the number of measurements.

E. Refinement

Once the association of each prediction with a measurement is accomplished, each IMM filter (track) is refined. Reliable state estimations of each object are computed with (15), while (14) enables each IMM to update the probabilities of their associated models.

IV. Results

A. Validation of Automatic Tracking on Synthetic Data

In order to assess the quality of our method and its suitability to biological data, we have generated sequences with artificial spots whose characteristics are as close as possible to fluorescent spots. The spots are represented by 3-D Gaussian shapes with different random covariance matrices in order to get different shapes of different sizes. For example of generated spots and of their detection, see Fig. 4.

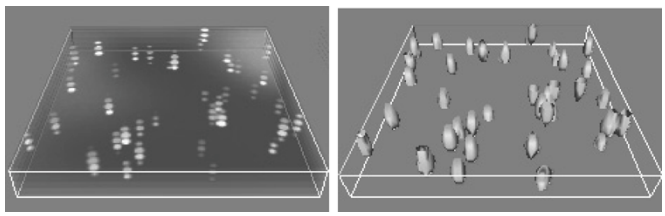

Fig. 4. Example of detection of synthetic spots. (a) Synthetic $100 \times 100 \times 5$ image stack with 40 synthetic spots and added Gaussian noise ($\sigma = 10$). Note the similarity with real microscopy data in Fig. 1. (b) Detected spots.

TABLE I
Influence of the Number of Spots on the Quality of Tracking. Table I Shows the Mean Results for the Analysis of Five Sequences of Thirty 100×100×10 Image Stacks for Each Spot Density. Results Are Expressed as the Percentage of True Positives and False Positives Given by the Tracking Procedure

Spot density	Single Model			IMM
	RW	FLE	SLE	
0.1	80 / 0	86.7 / 0	86.7 / 0	90 / 3.7
0.2	78.3 / 2.1	75 / 2.2	76.7 / 2.2	80 / 2.1
0.3	73.3 / 7.6	71.1 / 3.1	71.1 / 1.6	80 / 6.9
0.4	61.7 / 1.4	64.2 / 1.3	63.3 / 2.6	66.6 / 2.5

To test the robustness of the tracking algorithm to the density of spots, we included 10, 20, 30, or 40 spots in $100 \times 100 \times 10$ image stacks (the resulting spot density then being $d = 0.1$, 0.2, 0.3, and 0.4, for 10, 20, 30, and 40 spots) and generated five sequences of 30 time points for each condition (20 sequences in total). Here, the size of the test volumes was kept small in order to achieve relatively high densities of spots within tractable volumes. In each sequence, the spots were made to move randomly and their direction changed randomly at a random time of between one and five frames, with an additional random modification of the covariance matrix of the 3-D Gaussian shapes with time to make their aspect change. To simulate real world conditions, spots were allowed to temporarily aggregate and cross. Also, a simulated background was generated by using a mixture of Gaussians with high variance and white Gaussian noise was added to the sequence in order to represent the noise present in typical microscopy images. Finally, the image stacks have a lower resolution in the z direction to simulate the anisotropic resolution of 3-D microscopy images. Table I gives a summary of the influence of the density of spots within the same volume on the performances of the algorithm. The results show that even with a high density of spots the performances of the algorithm are satisfactory and that the IMM clearly outperforms the results achieved by using a KF with any of the three models (RW, FLE, or SLE) taken alone. Fig. 5 shows a synthetic sequence that was generated with 160 synthetic spots in a volume similar to the real data shown in Fig. 6, resulting in a similar spot density of $d = 0.25$. By applying the IMM filter to the data on this sequence, we could achieve a tracking with 85% of true positive

Fig. 5. Example of tracking 160 synthetic spots in a image sequence of 30 $100 \times 100 \times 5$ image stacks. The various types of simulated dynamics can be appreciated by the variety of the path.

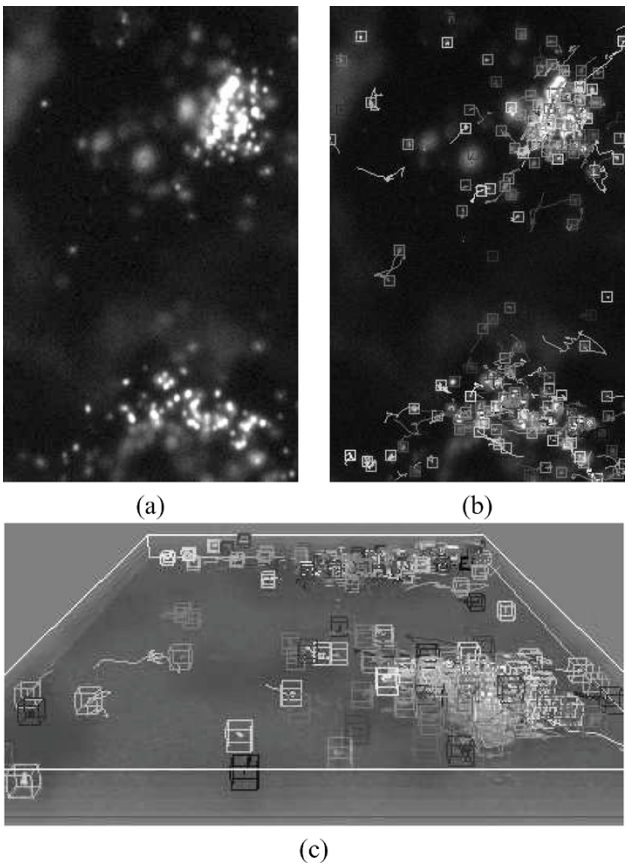

Fig. 6. Tracking of QDs in a 3-D+t sequence. (a) View of the original stack. (b) Two-dimensional view of the tracks. (c) Three-dimensional view of the tracks. This last view makes it clear that vesicle trajectories are not confined in a 2-D plane. Field of view is $50 \times 31 \times 2.5\,\mu$m.

and 6.1% of false positives, which is in good agreement with the results in Table I.

B. Tracking of QDs

We used our method to investigate the effect of the over-expression of the protein tau in the microtubule dependent transport of single vesicles in living cells. Tau is a microtubule associated protein (MAP) which regulates microtubule polymerization [34]. Independent experiments performed by a different team [28] have shown that tau does not alter the speed of moving vesicles but it affects the frequency of attachment and detachment of vesicles to the microtubules [28]. To monitor vesicle tracking we marked them with red emitting fluorescent inorganic CdSe/ZnS QDs and imaged them with time lapse 3-D fluorescence microscopy. A typical image stack acquired with the experimental setup described in Appendix I is presented in Fig. 6.

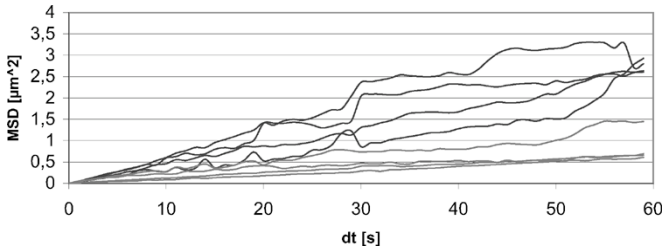

Fig. 7. Average MSD in four sequences of vesicles in nontreated cells (blue curves) and in four sequences of vesicles in cells transfected with tau (red curves). The curves show that in tau-transfected cells the motion is confined to a smaller volume than in the case of the nontransfected ones.

In the experiments, we monitored the dynamics of QD-containing vesicles over periods of several minutes without observing a decrease in the fluorescence emission. We compared the results obtained in nontreated cells and in cells transfected with tau-GFP for a total of about 30 cells in eight sequences (several cells can be found in one sequence). For each sequence, between 150 to 200 vesicles were tracked at the same time. For each trajectory, we computed the transport speed, the trajectory range R, defined as the largest distance separating the first and any other point in the sequence, and the mean-square displacement (MSD), defined as $\mathrm{MSD}(dt) = <[dr(dt)]^2>$, where $dr(dt)$ is the distance traveled in dt seconds. Fig. 7 shows the MSD curves corresponding to the movement of vesicles in cells for four sequences in the presence of tau (red) and for another four sequences in the absence of tau (blue) (each curve is the average of the MSDs for all vesicles in any of the sequences) and shows that in tau-transfected cells the motion is confined in a smaller volume than in the case of the nontransfected ones. From the data analysis, we found a mean speed of 0.12 and 0.11 μm/s and a mean trajectory range of 1.48 and 0.95 μm for nontreated and transfected cells, respectively. Therefore, we can confirm the result in [28] that tau does not affect the mean motor speed. On the contrary, as already suggested by Fig. 7, the overexpression of tau induces a reduction of almost a factor 1.6 for the value for the 3-D mean trajectory range. Also, from the values of the MSD curves corresponding to the two groups, we found the diameter of the mean diffusion volume to be 1.7 μm in absence of tau and 1.0 μm in presence of tau.

V. Conclusion

We have presented a method to detect and track fluorescence spots presenting different and switching movement types in 3-D+t live biological microscopic images. The method uses a shift-invariant 3-D wavelet transform for the detection of spots, an IMM algorithm with different transition models for the prediction and estimation of the state of the object and a data association method based on the maximum likelihood for establishing trajectories. We have shown on generated sequences and on real microscopy data sequences that this

multistage algorithm makes it possible to establish valid trajectories even in presence of a high density of spots. We have assessed the validity of our method by monitoring the effect of the overexpression of the protein tau in the microtubule dependent transport of single vesicles marked with QDs in living Hela cells and confirmed independent results that tau does not affect the mean motor speed. We now plan to apply our method to study the role of pathogen dynamics in the triggering of infectious diseases.

APPENDIX I
QDS SYNTHESIS AND MICROSCOPY SETTINGS

The synthesis of colloidal CdSe/ZnS nanoparticles is described in detail in a previous paper [35]. The hydrophobic particles were silanized with phosphonate silane as described in [36] to achieve water solubility. HeLa cells were grown in Dulbecco's modified minimal essential medium (Gibco, Cergy-Pontoise, France), supplemented with 10% fetal calf serum. For the experiment they were plated at a concentration of 7×10^4 cells/ml on 12.5 cm^2 round glass coverslip. After 24 h, the cells were transfected with the tau-GFP vector. Hydrophilic fluorescing nano-crystals with an emission wavelength of 637 nm were added to the medium to achieve a resulting concentration of 10-nM nanocrystals. The cells were then incubated for additional 4 h to allow the cells to completely ingest the nanocrystals and then rinsed two times with PBS to remove residual nano-crystals in the medium. Samples where observed with an inverted microscope (Leica) equipped with an $100\times$ oil-immersion objective and a 100-W mercury lamp. For every image, one channel in differential interference contrast mode and two individual channels in the fluorescence mode were recorded using the GFP filter set to image tau-GFP and a red filter set to image the QDs. The time-lapse sequences were recorded using the software Metamorph (Universal Imaging, WS). Nanocrystal subcellular traffic was tracked by recording on the red channel five z planes separated by 0.5 μm. For each plane, we used an integration time of 200 ms, which results in total acquisition time of 1 s for each z stack. For each cell, a total of 60 z stacks were acquired at an interval of 1 s.

ACKNOWLEDGMENT

The authors would like to thank B. Zhang and F. Ollivier for their help in implementing some of the algorithms described in this paper, as well as C. Zimmer for valuable comments and C. Durieux for help in cell culture and fluorescence labeling.

REFERENCES

[1] C. Zimmer, E. Labruyere, V. Meas-Yedid, N. Guillen, and J.-C. Olivo-Marin, "Segmentation and tracking of migrating cells in videomicroscopy with parametric active contours: a tool for cell-based drug testing," *IEEE Trans. Med. Imag.*, vol. 21, no. 10, pp. 1212–1221, Oct. 2002.

[2] D. McDonald, M. A. Vodicka, G. Lucero, T. M. Svitkina, G. G. Borisy, M. Emerman, and T. J. Hope, "Visualization of the intracellular behavior of HIV in living cells," *J. Cell. Biol.*, vol. 159, pp. 441–452, 2002.

[3] M. Lakadamyali, M. Rust, H. Babcock, and X. Zhuang, "Visualizing infection of individual influenza viruses," in *Proc. PNAS*, vol. 100, 2003, pp. 9280–9285.

[4] F. Frishneck, P. Baldacci, B. Martin, C. Zimmer, S. Thiberge, J.-C. Olivo-Marin, S. Shorte, and R. Ménard, "Imaging movement of malaria parasites during transmission by anopheles mosquitoes," *Cell. Microbiol.*, vol. 6, pp. 687–694, 2004.

[5] C. Murphy, R. Saffrich, J.-C. Olivo-Marin, A. Giner, W. Ansorge, T. Fotsis, and M. Zerial, "Dual function of rhoD in vesicular movement and cell motility," *Eur. J. Cell Biol.*, vol. 80, no. 6, pp. 391–398, 2001.

[6] D. Toomre, P. Keller, J. White, J.-C. Olivo, and K. Simons, "Dual-color visualization of trans-Golgi network to plasma membrane traffic along microtubules in living cells," *J. Cell. Sci.*, vol. 112, no. 1, pp. 21–33, 1999.

[7] M. Cheezum, W. Walker, and W. Guilford, "Quantitative comparison of algorithms for tracking single fluorescent particles," *Biophys. J.*, vol. 81, pp. 2378–2388, 2001.

[8] Y. Bar-Shalom and T. Fortmann, *Tracking and Data Association*. New York: Academic, 1988.

[9] Y. Bar-Shalom and W. D. Blair, *Multitarget-Multisensor Tracking Applications and Advances*. Norwood, MA: Artech House, Oct. 2000, vol. III.

[10] J. Apgar, Y. Tseng, E. Federov, M. Herwig, S. Almo, and D. Wirtz, "Multiple-particle tracking measurements of heterogeneities in solutions of actin filaments and actin bundles," *Biophys. J.*, vol. 79, pp. 1095–1106, 2000.

[11] J. Crocker and D. Grier, "Methods of digital video microscopy for colloidal studies," *J. Colloid Interf. Sci.*, vol. 179, pp. 298–310, 1996.

[12] W. Tvarusko, M. Bentele, T. Misteli, R. Rudolf, C. Kaether, D. L. Spector, H. H. Gerdes, and R. Eils, "Time-resolved analysis and visualization of dynamic process in living cells," in *Proc. PNAS*, vol. 96, 1999, pp. 7950–7955.

[13] A. Ponti, P. Vallotton, E. Salmon, C. Waterman-Storer, and G. Danuser, "Computational analysis of f-actin turnover in cortical actin meshworks using fluorescent speckle microscopy," *Biophys. J.*, vol. 84, pp. 3336–3352, 2003.

[14] P. Vallotton, A. Ponti, C. Waterman-Storer, E. Salmon, and G. Danuser, "Recovery, visualization, and analysis of actin and tubulin polymer flow in live cells: a fluorescent speckle microscopy study," *Biophys. J.*, vol. 85, pp. 1289–1306, 2003.

[15] F. Briquet-Laugier, C. Boulin, and J.-C. Olivo-Marin, "Analysis of moving biological objects in video microscopy sequences," *Proc. SPIE*, vol. 3642, pp. 1–11, 1998.

[16] A. Genovesio, B. Zhang, and J.-C. Olivo-Marin, "Tracking of multiple fluorescent biological objects in three dimensional video microscopy," in *Proc. IEEE Int. Conf. Image Processing*, vol. I, Barcelona, Spain, Sep. 2003, pp. 1105–1108.

[17] A. Genovesio and J.-C. O. Marin, "Interracting multiple model based method to track moving fluorescent biological spots," in *Proc. IEEE Int. Symp. Biomedical Imaging*, Arlington, VA, Apr. 2004, pp. 1239–1242.

[18] R. E. Kalman, "A new approach to linear filtering and prediction problems," *Trans. ASME J. Basic Eng.*, vol. 82, no. D, pp. 35–45, 1960.

[19] S. J. Julier, J. K. Uhlmann, and H. F. Durrant-Whyte, "A new approach for filtering nonlinear systems," in *Proc. Amer. Control Conf.*, Washington, DC, Jun. 1995, pp. 1628–1632.

[20] M. Isard and A. Blake, "Contour tracking by stochastic propagation of conditional density," in *Proc. Eur. Conf. Computer Vision*, vol. 1, 1996, pp. 343–356.

[21] A. Doucet, "On Sequential simulation-based methods for Bayesian filtering," Signal Processing Group, Dept. Eng., Univ. Cambridge, Cambridge, U.K., Tech. Rep. CUED/F-INFENG/TR.310, 1998.

[22] M. Arulampalam, S. Maskell, N. Gordon, and T. Clapp, "A tutorial on particle filters for online nonlinear/nongaussian bayesian tracking," *IEEE Trans. Signal Process.*, vol. 50, no. 2, pp. 174–188, Feb. 2002.

[23] H. A. P. Blom and Y. Bar-Shalom, "The interacting multiple model algorithm for systems with Markovian switching coefficients," *IEEE Trans. Autom. Control*, vol. 33, no. 8, pp. 780–783, Aug. 1988.

[24] H. A. P. Blom, "An efficient filter for abruptly changing systems," in *Proc. 23rd IEEE Conf. Decision Control*, Las Vegas, NV, Dec. 1984, pp. 656–658.

[25] T. Fortmann, Y. Bar-Shalom, and M. Scheffe, "Multi-target tracking using joint probabilistic data association," presented at the 19th IEEE Conf. Decision Control, Dec. 1980.

[26] D. B. Reid, "An algorithm for tracking multiple targets," *IEEE Trans. Autom. Control*, vol. AC-24, no. 12, pp. 843–854, Dec. 1979.

[27] I. J. Cox and S. L. Hingorani, "An efficient implementation of Reid's multiple hypothesis tracking algorithm and its evaluation for the purpose of visual tracking," *IEEE Trans. Pattern Anal. Mach. Intell.*, vol. 18, no. 2, pp. 138–150, Feb. 1996.

[28] B. Trinczek, A. Ebneth, E.-M. Mandelkow, and E. Mandelkow, "Tau regulates the attachement/detachement but not the speed of motors in microtubule-dependent transport of single vesicles and organelles," *J. Cell Sci.*, vol. 112, pp. 2355–2367, Jun. 1999.
[29] J.-C. Olivo-Marin, "Extraction of spots in biological images using multiscale products," *Pattern Recognit.*, vol. 35, no. 9, pp. 1989–1996, 2002.
[30] J.-L. Starck, F. Murtagh, and A. Bijaoui, *Image Processing and Data Analysis: The Multiscale Approach*. Cambridge, U.K.: Cambridge Unv. Press, 2000.
[31] M. A. T. Figueiredo and R. D. Nowak, "Wavelet-based image estimation: an empirical Bayes approach using Jeffrey's noninformative prior," *IEEE Trans. Image Process.*, vol. 10, no. 9, pp. 1322–1331, Sep. 2001.
[32] D. Donoho and I. Johnstone, "Ideal spatial adaptation via wavelet shrinkage," *Biometrika*, vol. 81, no. 3, pp. 425–455, 1994.
[33] R. Jonker and A. Volgenant, "A shortest augmenting path algorithm for dense and sparse linear assignment problems," *Computing*, vol. 38, pp. 325–340, 1987.
[34] N. Hirokawa, "Microtubule-organization and dynamics dependent on microtubule-associated proteins," *Curr. Opin. Cell Biol.*, vol. 6, pp. 74–81, 1994.
[35] T. Pellegrino, S. Kudera, T. Liedl, A. Javier, L. Mana, and W. J. Parak, "On the development of colloidal nanoparticles toward multifunctional structures and their possible use for biological applications," *Small*, vol. 1, pp. 48–63, 2005.
[36] D. Gerion, F. Pinaud, S. C. Williams, W. J. Parak, D. Zanchet, S. Weiss, and A. P. Alivisatos, "Synthesis and properties of biocompatible water-soluble silica-coated cdse/zns semiconductor quantum dots," *J. Phys. Chem. B*, vol. 105, no. 37, pp. 8861–8871, 2001.

Auguste Genovesio received the B.S. degree in applied mathematics, the B.S. degree in computer science, and the M.S. degree in artificial intelligence and pattern recognition from the Pierre et Marie Curie University, Paris, France, in 1998, 2000, and 2001, respectively, and the Ph.D. degree from the Universite Rene Descartes, Paris, in 2005.

He was with the Quantitative Image Analysis Unit, Institut Pasteur, Paris, from 2001 to 2005. He is now Head of the Image Mining Group, Institut Pasteur Korea, Seoul. His main research interests are in computer vision and its applications to the understanding and analysis of biological phenomena. His work has a special emphasis on 4-D biological particle tracking, Bayesian filtering, data association, and fast detection methods for high content screening.

Tim Liedl studied physics at the Ludwig Maximilian Universität München, Munich, Germany, and the Universidad de Sevilla, Sevilla, Spain. He received the Diploma in biological applications of colloidal semiconductor nanocrystals (Dr. W. J. Parak's group) from the Ludwig Maximilian Universität München in 2004. He is currently pursuing the Ph.D. degree (F. Simmel's group) at the Center for Nanoscience, Munich.

His research is focused on molecular machinery and self-assembly processes in nonequilibrium systems.

Valentina Emiliani received the Ph.D. degree in physics from the University La Sapienza, Rome, Italy, in 1996, with a dissertation on the investigation of tunneling effects in asymmetric double quantum wells.

From 1997 to 2000, she was with Prof. T. Elsaesser's group at the Max Born Institute, Berlin, Germany, as a postdoctorate working on the investigation of carrier transport in single quantum wire by low-temperature scanning near-field optical microscopy (SNOM). From 2000 to 2002, she was with Prof. M. Colocci's Laboratory at the European Laboratory for Nonlinear Spectroscopy, Florence, Italy, where she worked on the investigation of light propagation in disordered structure by SNOM. Since 2002, she has been with the Institute Jacques Monod (Dr. M. Coppey-Moisan's group), where she is investigating the role of mechanical force on the establishment of cell polarity by the use of the optical tweezers technique. In 2006, she joined the Neurophysiology and New Microscopy Laboratory, University Paris 5, Paris, France, directed by Dr. S. Charpak, where she leads a research team dedicated to the development of wave-front engineering microscopy. She is the coauthor of 40 publications in international journals.

Dr. Emiliani received the EURYI 2005 prize.

Wolfgang J. Parak received the Diploma in physics from the Technische Universität München, Munich, Germany, in 1997, and the Ph.D. degree from the Ludwig Maximilians Universität München (Prof. Dr. H. Gaub's group), in 1999, where he worked on cell-semiconductor hybrids.

From 2000 to 2002, he was a Postdoctoral Associate (Prof. P. Alivisatos' group) with the University of California, Berkely, where he worked on the synthesis of water-soluble fluorescent semiconductor nanoparticles. Since 2002, he has been an Assistant Professor with the Center for Nanoscience, Ludwig Maximilians Universität München, in the framework of an Emmy–Noether fellowship. His research is dedicated to the applications of colloidal nanoparticles in materials science and the life sciences. In 2006, he joined the Universität Leipzig as a Professor.

Maïté Coppey-Moisan is a Research Director with INSERM and Group Leader at the Institut Jacques Monod, Paris, France, where she is also Head of the Cell Imaging and Nano Manipulation Facilities. Her scientific background is in biophysics and cell biology. Her group is interested in the problem of how mechanical tensions and 3-D extracellular architecture are involved in cell shape and polarization. Her current work is aimed at using fluorescent biosensors and two-photon microscopy coupled to FLIM and optical tweezers to relate cellular shape changes induced by mechanochemical gradients to molecular mechanisms. Dynamics of the cytoskeletton and of the related enzymatic activities and proteins are investigated by FRAP, SPT, and FRET.

Jean-Christophe Olivo-Marin (M'93–SM'05) received the Ph.D. and the "Habilitation à Diriger des Recherches" degrees from the Institut d'Optique Théorique et Appliquée, University of Paris, Orsay, France, in 1989 and 1998, respectively.

He is Head of the Quantitative Image Analysis Group, Institut Pasteur, Paris. From 2004 to May 2005, he held a joint appointment as Chief Technology Officer at the Institut Pasteur Korea, Seoul. From 1990 to 1998, he was a Staff Scientist at the European Molecular Biology Laboratory, Heidelberg, Germany. His research interests are in image processing and computer vision applied to biological image analysis, with special emphasis on multiresolution processing, cell and particle tracking, and multidimensional microscopy.

Dr. Olivo-Marin is a member of the IEEE SPS TC on Bio Image and Signal Processing, SPIE, and the Pattern Recognition Society.